THE JOURNAL OF PHYSICAL CHEMISTRY LETTERS
A JOURNAL OF THE AMERICAN CHEMICAL SOCIETY

pubs.acs.org/JPCL Letter

Piezovoltaics from PdH_x

Yida Wang, Guangwei Che, Xin Yang, Jie Zheng,* Youyu Lin, Haiyan Zheng, Kuo Li,* and Ho-kwang Mao

Cite This: *J. Phys. Chem. Lett.* 2023, 14, 3168−3173 Read Online

ACCESS | Metrics & More | Article Recommendations | Supporting Information

ABSTRACT: Metal hydrides have wide applications in energy science. A large pressure gradient propels the hydrogen atoms out. A piezovoltaic device, a pressure gradient-driven battery, can therefore be realized when the migrations of protons and electrons are separated by different conductors. Here we investigate the piezovoltaic performance of PdH_x with various proton conductors as electrolytes and experimentally detect an output current of $\lesssim$40 nA and a voltage of ∼0.8 V for a 3 μg sample. We also demonstrate the escape of hydrogen atoms from a palladium lattice under an increasing pressure gradient using X-ray diffraction. The relationship between piezovoltaics (chemical process) and piezoelectricity (physical process) is like that between a chemical battery and a capacitor. Our work demonstrates the piezovoltaic application of metal hydrides and provides a new way to convert mechanical energy into electrical energy.

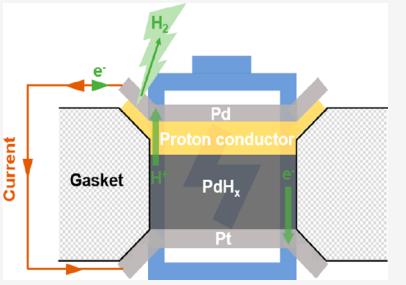

Metal hydrides (MHs) are in focus due to their wide applications in energy science as hydrogen storage materials,[1−3] heat storage materials,[4−7] additives in energetic materials,[8−10] and electrode materials in batteries. In electrochemistry, it is an inviting anode material in lithium-ion batteries due to its weak polarization, high theoretical capacity, and suitable working potential.[11−13] It also plays a significant role in nickel−metal hydride batteries, acting as an active negative electrode material.[14,15] Recently, a large number of hydrogen-rich metal hydrides were synthesized or predicted under high pressure, like CaH_6,[16] LiH_8,[17] BeH_2,[18] Li_2MgH_{16},[19] YH_3,[20] PbH_8,[21] AsH_8,[22] LaH_{10},[23] etc. High pressure not only enriches the variety of metal hydrides with higher hydrogen content but also significantly changes the thermodynamics of metal hydrides, as manifested by their synthetic reactions and diverse phase transitions under applied pressure.[24−26] Thermodynamically, applying pressure increased the Gibbs free energy and the chemical equilibrium moves to the lower-free energy side. Considering an isothermal process ($dT = 0$), the pressure-induced change in the Gibbs free energy (ΔG) for substance A is expressed as $\Delta G_A|_{P_0}^{P_1} = \int_{P_0}^{P_1} dG = \int_{P_0}^{P_1} V_A\, dP - \int_{P_0}^{P_1} S_A\, dT = \int_{P_0}^{P_1} V_A\, dP$, as represented by the area covered by the orange line in Scheme 1. For an A to B process happening at a high static pressure P_1, $\Delta G_{r,P_1} = \Delta G_{r,P_0} + \Delta G_B|_{P_0}^{P_1} - \Delta G_A|_{P_0}^{P_1}$, where $\Delta G_{r,P_0}$ is the ΔG under P_0 (∼0 GPa), and the ΔG contributed by external pressure ($\Delta G_B|_{P_0}^{P_1} - \Delta G_A|_{P_0}^{P_1}$) is represented by the difference in the area covered by the orange line and that covered by the green line in Scheme 1.

Following the law of thermodynamics, if a pressure gradient (PG) is involved, some components like hydrogen in the sample chamber under high pressure (HP) can be pushed out into ambient pressure (AP) through and/or bypass the gasket,

Scheme 1. Gibbs Free Energy Changes Contributed by Applied Pressure

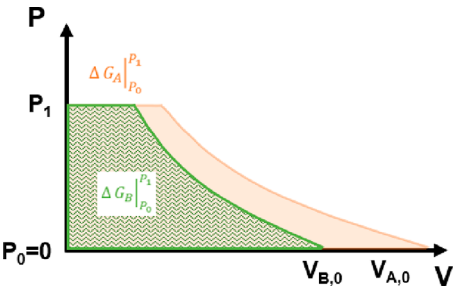

and then the Gibbs free energy change caused by the leaked atoms should be accounted. For an $A(P_1) = B(P_0)$ process, the expected B is subjected to a pressure gradient from high pressure P_1 to low pressure P_0 [$\Delta G_{PG} = (\Delta G_{r,P_0} + \Delta G_B|_{P_0}^{P_1} - \Delta G_A|_{P_0}^{P_1}) + \Delta G_B|_{P_0}^{P_1} = \Delta G_{r,P_0} - \Delta G_A|_{P_0}^{P_1}$]; hence, $|\Delta G_{PG}| \gg |\Delta G_{r,P_1}|$, indicating a pressure gradient affords a much higher thermodynamic potential to trigger reactions (the whole area covered by the orange line in Scheme 1). We calculated that the enthalpy will decrease by ∼1 eV when 0.5 H_2 molecule is released from 40 GPa to ambient pressure at 0 K (96.5 kJ/mol of $0.5H_2$, or 26.8 kWh/kg of H_2). This is regarded as a gauge

Received: February 17, 2023
Accepted: March 20, 2023
Published: March 24, 2023

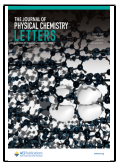

https://doi.org/10.1021/acs.jpclett.3c00464
J. Phys. Chem. Lett. 2023, 14, 3168−3173

(HP H_2 ruler)[27] for comparing to the enthalpy changes of various hydrides and judging whether the dehydrogenation reaction can occur spontaneously. Theoretically, driven by a pressure difference of 40 GPa, PdH can release as much as ~250 Wh/kg (detailed in the Supporting Information), which is comparable to or even exceeds that of commercial lithium-ion batteries.[28]

Experimentally, such a dehydrogenation was realized by compressing MnOOH to tens of gigapascals using a diamond anvil cell (DAC) with Nafion as the electrolyte affording the pressure gradient.[27] It expels hydrogen into environment and converts mechanical energy into electrical energy, which is a pressure gradient-driven battery (PGDB). The output short-circuit current was ~0.7 nA at the maximum, but no output voltage was detected due to the low proton conductance under high pressure and limited thermodynamic driving force. In this work, by employing PdH_x as the anode, we successfully realized a more powerful piezovoltaic device PdH_x-Pd PGDB with an open-circuit voltage of ≲0.8 V and demonstrated the escape of hydrogen from the palladium lattice under an increasing pressure gradient by X-ray diffraction (XRD). In this way, pressure gradient drives the migration of hydrogen, converts mechanical energy into electrical energy, and demonstrates an unprecedented application of metal hydride in energy science.

A Pd (cathode, PG)|proton conductor (electrolyte, PG)|PdH_x (anode, HP)|Pt (wire, PG) PGDB is prepared with different proton conductors as shown in Scheme 2, where PG and HP represent a pressure gradient and high pressure, respectively. PdH_x [the morphologies were assessed by scanning electron microscopy (SEM) (see Figure S2)] is the anode that provides protons to the electrolyte (proton conductors) on the top side, which transport the protons to the palladium electrode (cathode) but block electrons. Here potassium hydroxide (KOH), phosphomolybdic acid hydrate (PMA), and phosphotungstic acid hydrate (PTA) are used as electrolytes, as all of them have robust structures under applied pressure. On the bottom side of PdH_x, platinum foil transports electrons to ambient pressure but blocks protons. The electrons are transferred through the circuit and recombine with protons at the cathode.

Scheme 2. Schematic Plot of a PdH_x-Pd Pressure Gradient-Driven Battery

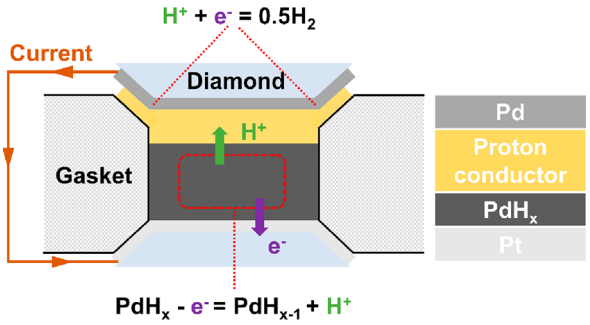

First, we measured the short-circuit current of the Pd (PG)|KOH (PG)|PdH_x (HP)|Pt (PG) PGDB up to 35 GPa, with KOH as the electrolyte. A current of tens of nanoamperes was detected in compression and decompression processes following the normal connection (purple line in Figure 1; see panels a and c of Figure S3 for complete initial data varying with time), with no notable current detected in the reverse connection (Figure S3b,d, sensitivity test in ref 27). Considering the mass of PdH_x is only 3 μg, this corresponds to ~10 A/kg of sample, which is a big improvement compared to that of the previous PGDB using MnOOH.

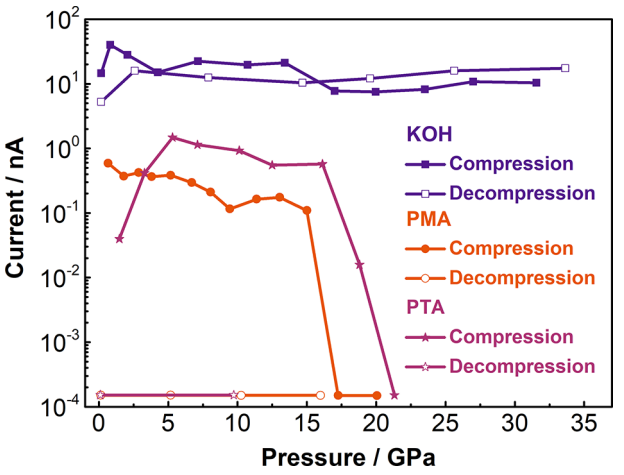

Figure 1. Short-circuit current of the Pd (PG)|electrolyte (PG)|PdH_x (HP)|Pt (PG) PGDB, with KOH, PMA, and PTA as electrolytes under high pressure in the normal connection.

Obviously, this improvement is closely related to the high hydrogen (proton + electron) conductivity of PdH_x. On the contrary, to investigate the effect of different electrolytes, PMA and PTA were tested as electrolytes. For PMA, a current of ~0.3 nA was detected upon compression until its failure at 17 GPa (orange line in Figure 1; see Figure S4a for complete initial data varying with time), with no notable current with decompression progress (Figure S4c). The failure of PMA was attributed to an irreversible transition, where the resistance decreased sharply from 60 to 2 kΩ at 17 GPa, as proven by electrochemical impedance spectroscopy of PMA in Figure S5. This indicates that the electronic conductivity of PMA also increases above 17 GPa, and thus, PMA is no longer suitable as an electrolyte. The performance of PTA (claret line in Figure 1; see Figure S6 for complete initial data varying with time) is similar to that of PMA with a current of ~1 nA below 19 GPa. PTA also experienced an irreversible damage above ~18 GPa, which led to the failure of the PGDB, as proven by the *in situ* high-pressure Raman spectra in Figure S7. The good performances of KOH, PMA, and PTA in PGDB suggest that the PGDB model is widely applied, compatible with many electrolytes. On the contrary, the different outputs also indicate that the electrolyte is a key component in the PGDB, which is the bottleneck to the transport of ions.

Then we investigated the open-circuit voltage of PGDB, which is a more important parameter in electrochemistry. Using KOH and Nafion as electrolytes, voltages of ≲0.8 and ≲0.6 V, respectively, were detected in the PdH_x-Pd PGDB upon compression (Figure 2a,b). The time-dependent voltages are displayed in Figure S8, which shows that the voltage did not change significantly during our measurement. During decompression, the voltages were also stably detected with similar values (Figure 2b).

By dividing the open-circuit voltage by the short-circuit current, we obtained the inner resistance. The typical value is ~30 MΩ (40 MΩ under 5 GPa and 27 MΩ under 11 GPa), and the expected maximum output power is 2.6 nW, when the

https://doi.org/10.1021/acs.jpclett.3c00464
J. Phys. Chem. Lett. 2023, 14, 3168−3173

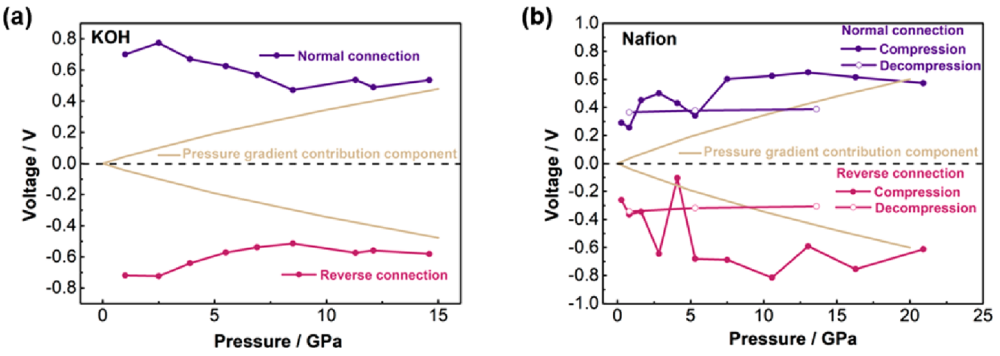

Figure 2. (a) Open-circuit voltage of the Pd (PG)|KOH (PG)|PdH_x (HP)|Pt (PG) PGDB upon compression following the normal (above the dashed line) and reverse connection (below the dashed line). The khaki line represents the contribution component of voltage by pressure gradient. (b) Open-circuit voltage of the Pd (PG)|Nafion (PG)|PdH_x (HP)|Pt (PG) PGDB.

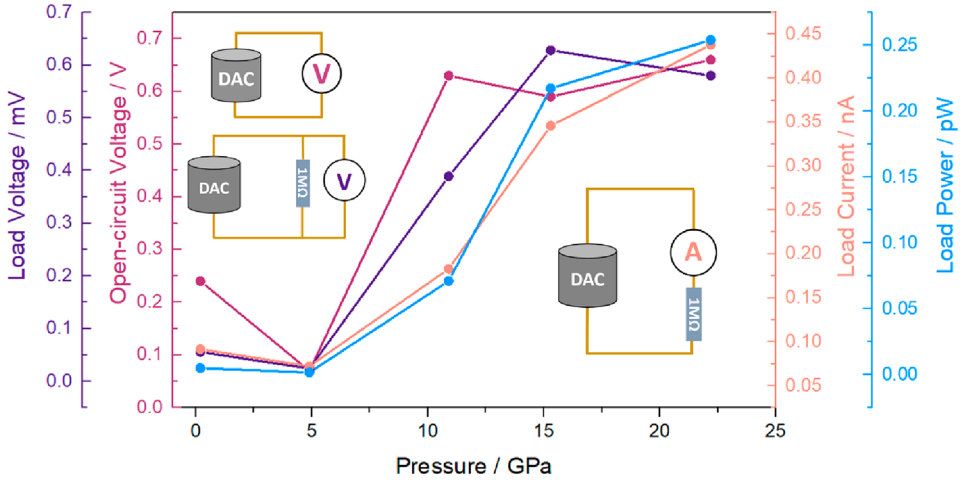

Figure 3. Voltage on load, open-circuit voltage, and output current of the Pd (PG)|Nafion (PG)|PdH_x (HP)|Pt (PG) PGDB during compression following the normal connection.

resistance of the load is the same as the inner resistance. To test the output power, a constant resistor of 1 MΩ was connected to the circuit as a load for the Pd (PG)|Nafion (PG)|PdH_x (HP)|Pt (PG) PGDB, and the output voltage and current were measured separately (circuit in the inset of Figure 3). The open-circuit voltages were also measured for reference and are in agreement with the previous results. The output power reaches a maximum of 0.25 pW at 22 GPa. These significant electrical signals reveal that metal hydrides release electrical energy during dehydrogenation following the mechanism of the PGDB.

Then we carefully investigated the origin of the detected voltages. When the hydrogen was absorbed in the cathode or anode, the electrochemical reactions include $Pd + \delta H^+ + \delta e^- = PdH_\delta$ (cathode) and $PdH_x - \delta e^- = PdH_{x-\delta} + \delta H^+$ (anode). The voltage results from two sources. The first is the intrinsic electrochemical potential difference between Pd and PdH_x, or the asymmetry of this "symmetric" battery, and the second is the pressure gradient-introduced electrochemical potential (khaki line in Figure 2). At low pressure, the intrinsic potential is the dominant contributor of voltage. Because a higher hydrogen content results in a more negative electrode potential, the PdH_x anode released an electron to the circuit and H^+ to the electrolyte, and the Pd cathode absorbed H^+ and an electron in a reverse reaction. The exact voltage is difficult to calculate, because the reaction details and the hydrogen content on or near the surface are unknown. The investigations[29,30] provided the thermodynamic electrode potentials. From that, we found the voltage between our two electrodes ($PdH_{0.57}$ and Pd) should be ~0.75 V, which is consistent with our experimental data (0.7 V) at 1 GPa [the lowest pressure (Figure 2a)]. However, because the changes in surface potential were closely related to surface defects as indicated by the atomic force microscopy experiment,[29] the direct comparison with our results needs to be investigated further.

Under higher pressure, the voltage contributed by the pressure gradient was enhanced, while the results from the intrinsic composition difference were suppressed. If the total chemical equation PdH_x (HP) + Pd (AP) = $PdH_{x-\delta}$ (HP) + PdH_δ (AP) is broken into three equations

$$PdH_x\,(HP) = PdH_{x-\delta}\,(HP) + 0.5\delta H_2\,(HP) \quad (1)$$

$$0.5\delta H_2\,(HP) = 0.5\delta H_2\,(AP) \quad (2)$$

$$Pd\,(AP) + 0.5\delta H_2\,(AP) = PdH_\delta\,(AP) \quad (3)$$

obviously the ΔG contributed by the composition difference between reactions 1 and 3 is suppressed under high pressure, because eq 1 is not favored under high pressure and eq 3 is unchanged. Then the ΔG_r of the total reaction is mainly contributed by eq 2. We calculated the corresponding voltage of eq 2 by the Nernst equation from the H-ruler data mentioned in ref 19 (khaki line in Figure 2) and found the

https://doi.org/10.1021/acs.jpclett.3c00464
J. Phys. Chem. Lett. 2023, 14, 3168−3173

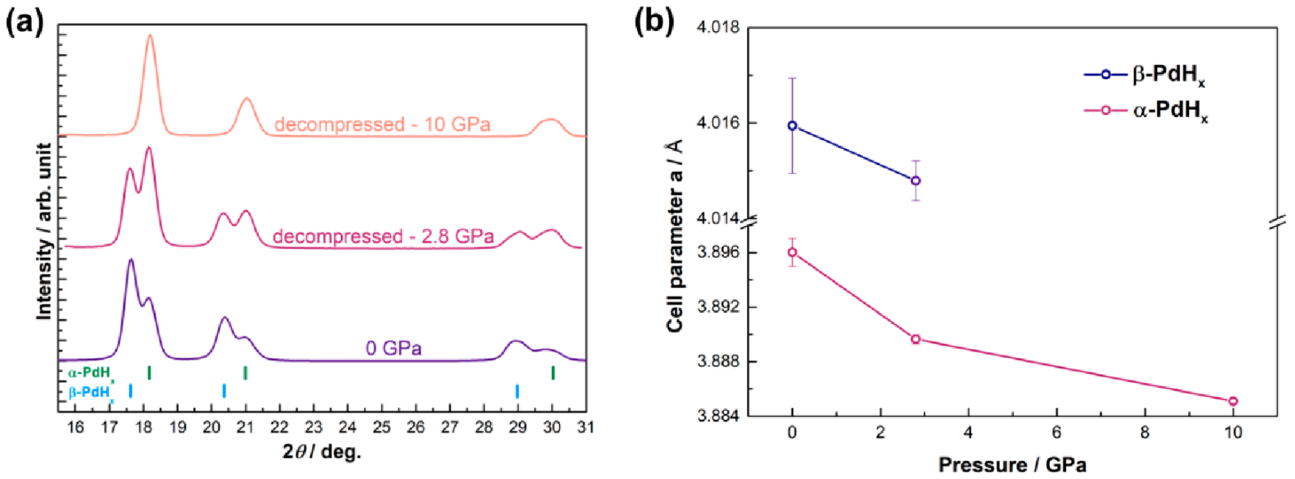

Figure 4. (a) XRD patterns of the same PdH_x sample decompressed from high pressure (λ = 0.7107 Å). (b) Variations in cell parameter a of PdH_x as a function of pressure.

detected voltage was supplied entirely by the pressure gradient under relatively high pressure.

For comparison, we also investigated the whole electrochemical process under static pressure. We excluded the pressure gradient effect by loading Pd powder, Nafion film, and PdH_x powder into the insulated sample chamber from top to bottom between two Pt electrodes. The materials completely filled the chamber without overflow, bringing no notable pressure gradient on Pd, Nafion, or PdH_x and forming the Pt (PG)|Pd (HP)|Nafion (HP)|PdH_x (HP)|Pt (PG) battery. The measurement showed no meaningful current or voltage signals (Figure S9). This indicated the reaction cannot proceed under static pressure and demonstrated the significance of the pressure gradient once more.

An XRD experiment showed that the pressure gradient is an indispensable driving force. To probe the dehydrogenation reactions of PdH_x directly under a pressure gradient, we performed XRD of the same PdH_x sample decompressed from high pressure. To generate the pressure gradient for hydrogen transfer, the sample was loaded into a precompressed but unperforated T301 stainless steel gasket completely covered by a Nafion film. The PdH_x sample (precompressed to 350 MPa) was compressed up to 10 GPa, and the XRD patterns decompressed from applied pressure are displayed in Figure 4a. The sample contains both β-PdH_x and α-PdH_x ($Fm\bar{3}m$; for β-PdH_x, a = 4.016 Å; for α-PdH_x, a = 3.896 Å).[31] After decompression from 2.8 GPa, the two phases still coexisted, with the H-rich phase β-PdH_x significantly decreased, while the sample decompressed from 10 GPa contained only α-PdH_x. On LeBail refinement of PdH_x at ambient pressure (Figure S10a), in addition to the change in the component proportion, the cell parameter decreased in both phases with an increase in pressure (Figure 4b). This is direct evidence of the dehydrogenation reaction under a pressure gradient. The limited amount of residual hydrogen indicates the intrinsic electrochemical potential difference between Pd and PdH_x is not dominating any more above a high pressure like 10 GPa.

In conclusion, we created a piezovoltaic device by driving the dehydrogenation of metal hydride PdH_x in PGDB with an output voltage of ~0.8 V and a current of ~10 A/kg. This piezovoltaic device uses a pressure gradient as the driving force, and PdH_x decomposes via a dehydrogenation reaction. This is an electrochemical process in contrast to piezoelectricity, where the piezoelectric material[32−34] is polarized under an external force with positive and negative charges concentrated on two opposite surfaces (physical process). The relationship between the piezovoltaic and piezoelectricity is just like that between the chemical battery, which includes electrochemical reaction, and the capacitor, which involves only the physical process of charge separation. We also directly revealed that the hydrogen atoms escaped from the palladium lattice under an increasing pressure gradient with an XRD experiment. Our work demonstrates an unprecedented piezovoltaic application of metal hydride as a PGDB, which makes metal hydride not only a container for hydrogen storage but also a battery "fuel" for generating electricity in the process of releasing hydrogen.

■ ASSOCIATED CONTENT

Supporting Information

The Supporting Information is available free of charge at https://pubs.acs.org/doi/10.1021/acs.jpclett.3c00464.

Details of the preparation of materials, measurement methods, and supplementary figures, including Materials and chemicals (section S1), preparation of PdH_x (section S2), electrical measurements (section S3), X-ray diffraction (section S4), water content of electrolytes (Figure S1), SEM image of PdH_x (Figure S2), short-circuit current of the Pd (PG)|KOH (PG)|PdH_x (HP)|Pt (PG) PGDB (Figure S3), short-circuit current of the Pd (PG)|PMA (PG)|PdH_x (HP)|Pt (PG) PGDB (Figure S4), resistance of PMA under external pressure (Figure S5), short-circuit current of the Pd (PG)|PTA (PG)|PdH_x (HP)|Pt (PG) PGDB (Figure S6), Raman spectra of PTA under applied pressure (Figure S7), open-circuit voltage of the Pd (PG)|KOH (PG)|PdH_x (HP)|Pt (PG) and Pd (PG)|Nafion (PG)|PdH_x (HP)|Pt (PG) PGDBs (Figure S8), open-circuit voltage and short-circuit current of the Pt (PG)|Pd (HP)|Nafion (HP)|PdH_x (HP)|Pt (PG) PGDB (Figure S9), and XRD patterns of PdH_x (Figure S10) (PDF)

Transparent Peer Review report available (PDF)

https://doi.org/10.1021/acs.jpclett.3c00464
J. Phys. Chem. Lett. 2023, 14, 3168−3173

AUTHOR INFORMATION

Corresponding Authors

Kuo Li − *Center for High Pressure Science and Technology Advanced Research, 100193 Beijing, China;* orcid.org/0000-0002-4859-6099; Email: likuo@hpstar.ac.cn

Jie Zheng − *Beijing National Laboratory for Molecular Sciences, College of Chemistry and Molecular Engineering, Peking University, 100871 Beijing, China;* orcid.org/0000-0003-1817-6357; Email: zhengjie@pku.edu.cn

Authors

Yida Wang − *Center for High Pressure Science and Technology Advanced Research, 100193 Beijing, China*

Guangwei Che − *Center for High Pressure Science and Technology Advanced Research, 100193 Beijing, China*

Xin Yang − *Center for High Pressure Science and Technology Advanced Research, 100193 Beijing, China*

Youyu Lin − *Beijing National Laboratory for Molecular Sciences, College of Chemistry and Molecular Engineering, Peking University, 100871 Beijing, China*

Haiyan Zheng − *Center for High Pressure Science and Technology Advanced Research, 100193 Beijing, China;* orcid.org/0000-0002-4727-5912

Ho-kwang Mao − *Center for High Pressure Science and Technology Advanced Research, 100193 Beijing, China*

Complete contact information is available at: https://pubs.acs.org/10.1021/acs.jpclett.3c00464

Notes

The authors declare no competing financial interest.

ACKNOWLEDGMENTS

The authors greatly appreciate the financial support from the National Natural Science Foundation of China (NSFC) (Grants 22022101, 21875006, and 21771011) and National Key Research and Development Program of China (Grant 2019YFA0708502).

REFERENCES

(1) Eberle, U.; Felderhoff, M.; Schüth, F. Chemical and Physical Solutions for Hydrogen Storage. *Angew. Chem., Int. Ed.* **2009**, *48*, 6608−6630.

(2) Sakintuna, B.; Lamari-Darkrim, F.; Hirscher, M. Metal Hydride Materials for Solid Hydrogen Storage: A Review. *Int. J. Hydrogen Energy* **2007**, *32*, 1121−1140.

(3) Huang, Y.; Cheng, Y.; Zhang, J. A Review of High Density Solid Hydrogen Storage Materials by Pyrolysis for Promising Mobile Applications. *Ind. Eng. Chem. Res.* **2021**, *60*, 2737−2771.

(4) Izhvanov, L. A.; Solovey, A. I.; Frolov, V. P.; Shanin, Y. I. Metal Hydride Heat Pump—New Type of Heat Converter. *Int. J. Hydrogen Energy.* **1996**, *21*, 1033−1038.

(5) Altinisik, K.; Veziroglu, T. N. Metal Hydride Heat Pumps. *Int. J. Energy Res.* **1991**, *15*, 549−560.

(6) Lototskyy, M.; Satya Sekhar, B.; Muthukumar, P.; Linkov, V.; Pollet, B. G. Niche Applications of Metal Hydrides and Related Thermal Management Issues. *J. Alloys Compd.* **2015**, *645*, S117−S122.

(7) Malleswararao, K.; Dutta, P.; Murthy S, S. Applications of Metal Hydride Based Thermal Systems: A Review. *Appl. Therm. Eng.* **2022**, *215*, 118816.

(8) Cheng, Y.; Ma, H.; Liu, R.; Shen, Z. Explosion Power and Pressure Desensitization Resisting Property of Emulsion Explosives Sensitized by MgH_2. *J. Energy Mater.* **2014**, *32*, 207−218.

(9) Yao, Y.; Cheng, Y.; Zhang, Q.; Xia, Y.; Hu, F.; Wang, Q.; Chen, Y. Explosion Temperature Mapping of Emulsion Explosives Containing TiH_2 Powders with the Two-color Pyrometer Technique. *Def. Technol.* **2022**, *18*, 1834−1841.

(10) Fang, H.; Guo, X.; Shi, L. C.; Han, K.; Nie, J.; Wang, S.; Wu, C.; Deng, P. The Effects of TiH_2 on the Thermal Decomposition Performances of Ammonium Perchlorate-based Molecular Perovskite (DAP-4). *J. Energy Mater.* **2023**, *41*, 86−98.

(11) Liu, C.; Sun, J.; Zheng, P.; Jiang, L.; Liu, H.; Chai, J.; Liu, Q.; Liu, Z.; Zheng, Y.; Rui, X. Recent Advances of Non-lithium Metal Anode Materials for Solid-state Lithium-ion Batteries. *J. Mater. Chem. A* **2022**, *10*, 16761−16778.

(12) Pang, Y.; Liu, Y.; Yang, J.; Zheng, S.; Wang, C. Hydrides for Solid-state Batteries: A Review. *Mater. Today Nano* **2022**, *18*, 100194.

(13) Cheng, Q.; Sun, D.; Yu, X. Metal Hydrides for Lithium-ion Battery Application: A Review. *J. Alloys Compd.* **2018**, *769*, 167−185.

(14) Taniguchi, A.; Fujioka, N.; Ikoma, M.; Ohta, A. Development of Nickel/Metal-hydride Batteries for EVs and HEVs. *J. Power Sources* **2001**, *100*, 117−124.

(15) Yasuoka, S.; Magari, Y.; Murata, T.; et al. Development of High-capacity Nickel-metal Hydride Batteries using Superlattice Hydrogen-absorbing Alloys. *J. Power Sources* **2006**, *156*, 662−666.

(16) Wang, H.; Tse, J. S.; Tanaka, K.; Iitaka, T.; Ma, Y. Superconductive Sodalite-like Clathrate Calcium Hydride at High Pressures. *Proc. Natl. Acad. Sci. U. S. A.* **2012**, *109*, 6463−6466.

(17) Xie, Y.; Li, Q.; Oganov, A. R.; Wang, H. Superconductivity of Lithium-Doped Hydrogen under High Pressure. *Acta Crystallogr., Sect. C* **2014**, *70*, 104−111.

(18) Vajeeston, P.; Ravindran, P.; Kjekshus, A.; Fjellvag, H. Structural Stability of BeH_2 at High Pressures. *Appl. Phys. Lett.* **2004**, *84*, 34−36.

(19) Sun, Y.; Lv, J.; Xie, Y.; Liu, H.; Ma, Y. Route to a Superconducting Phase above Room Temperature in Electron-Doped Hydride Compounds under High Pressure. *Phys. Rev. Lett.* **2019**, *123*, 97001.

(20) Li, Y.; Hao, J.; Liu, H.; Tse, J. S.; Wang, Y.; Ma, Y. Pressure-stabilized Superconductive Yttrium Hydrides. *Sci. Rep.* **2015**, *5*, 9948.

(21) Chen, B.; Conway, L. J.; Sun, W.; Kuang, X.; Lu, C.; Hermann, A. Phase Stability and Superconductivity of Lead Hydrides at High Pressure. *Phys. Rev. B* **2021**, *103*, 035151.

(22) Fu, Y.; Du, X.; Zhang, L.; Peng, F.; Zhang, M.; Pickard, C. J.; Needs, R. J.; Singh, D. J.; Zheng, W.; Ma, Y. High-pressure Phase Stability and Superconductivity of Pnictogen Hydrides and Chemical Trends for Compressed Hydrides. *Chem. Mater.* **2016**, *28*, 1746−1755.

(23) Liu, H.; Naumov, I. I.; Hoffmann, R.; Ashcroft, N. W.; Hemley, R. J. Potential High-T_c Superconducting Lanthanum and Yttrium Hydrides at High Pressure. *Proc. Natl. Acad. Sci. U. S. A.* **2017**, *114*, 6990.

(24) Lv, H.; Chen, M.; Feng, Y.; Li, W.; Zhong, G.; Yang, C. Superconductivity of Light-Metal Hydrides. *J. Chin. Chem. Soc.* **2019**, *66*, 1246−1256.

(25) Bronger, W.; Auffermann, G. New Ternary Alkali-Metal-Transition-Metal Hydrides Synthesized at High Pressures: Characterization and Properties. *Chem. Mater.* **1998**, *10*, 2723−2732.

(26) Hou, H.; Pan, Y.; Bai, G.; Li, Y.; Murugadoss, V.; Zhao, Y. High-throughput Computing for Hydrogen Transport Properties in ε-ZrH_2. *Adv. Compos. Hybrid Mater.* **2022**, *5*, 1350−1361.

(27) Wang, Y.; Yang, X.; Tang, X.; Wang, X.; Li, Y.; Lin, X.; Dong, X.; Yang, D.; Zheng, H.; Li, K.; Mao, H. K. Pressure Gradient Squeezing Hydrogen out of MnOOH: Thermodynamics and Electrochemistry. *J. Phys. Chem. Lett.* **2021**, *12*, 10893−10898.

(28) Li, J.; Fleetwood, J.; Hawley, W. B.; Kays, W. From Materials to Cell: State-of-the-art and Prospective Technologies for Lithium-ion Battery Electrode Processing. *Chem. Rev.* **2022**, *122*, 903−956.

(29) Dus, R.; Nowicka, E.; Nowakowski, R. The Response of Work Function of Thin Metal Films to Interaction with Hydrogen. *Acta Phys. Pol., A* **2008**, *114*, S29−S47.

(30) Dus, R. Hydrogen Adsorption and Absorption on Evaporated Palladium Films: Study by Surface Potential Measurements. *Surf. Sci.* **1974**, *42*, 324−328.

(31) Akiba, H.; Kofu, M.; Kobayashi, H.; Kitagawa, H.; Ikeda, K.; Otomo, T.; Yamamuro, O. Nanometer-Size Effect on Hydrogen Sites in Palladium Lattice. *J. Am. Chem. Soc.* **2016**, *138*, 10238−10243.
(32) Li, G.; Li, J.; Li, Z.; Zhang, Y.; Zhang, X.; Wang, Z.; Han, W.; Sun, B.; Long, Y.; Zhang, H. Hierarchical PVDF-HFP/ZnO Composite Nanofiber−based Highly Sensitive Piezoelectric Sensor for Wireless Workout Monitoring. *Adv. Compos. Hybrid Mater.* **2022**, *5*, 766−775.
(33) Li, J.; Zhu, X.; Zhang, X.; Zhang, H. Aging Effects on Resonance Frequency of $Pb(Ti_{0.52}Zr_{0.48})O_3$ Piezoelectric Ceramics for Power Ultrasonic Transducers. *Adv. Compos. Hybrid Mater.* **2021**, *4*, 806−814.
(34) Wang, Z.; Song, J. Piezoelectric Nanogenerators Based on Zinc Oxide Nanowire Arrays. *Science* **2006**, *312*, 242−246.

https://doi.org/10.1021/acs.jpclett.3c00464
J. Phys. Chem. Lett. 2023, 14, 3168−3173